

# Control of the helicity of high-order harmonics generated by bicircular field

D. B. Milošević<sup>1,2,3</sup>

<sup>1</sup>*Faculty of Science, University of Sarajevo, Zmaja od Bosne 35, 71000 Sarajevo, Bosnia and Herzegovina*

<sup>2</sup>*Academy of Sciences and Arts of Bosnia and Herzegovina, Bistrik 7, Sarajevo, Bosnia and Herzegovina*

<sup>3</sup>*Max-Born-Institut, Max-Born-Strasse 2a, 12489 Berlin, Germany*

(Dated: August 30, 2018)

High-order harmonics generated by bicircular laser field have helicities which alternate between +1 and -1. In order to generate circularly polarized high-harmonic pulses, which are important for applications, it is necessary to achieve asymmetry in emission of harmonics having opposite helicities. We theoretically investigated a wide range of bicircular field component intensities and found areas where both the harmonic intensity is high and the helicity asymmetry is large. We investigated the cases of  $\omega-2\omega$  and  $\omega-3\omega$  bicircular fields and atoms having the  $s$  and  $p$  ground states, exemplified by He and Ne atoms, respectively. We have shown that for He atoms strong high harmonics having positive helicity can be generated using  $\omega-3\omega$  bicircular field with a much stronger second field component. For Ne atoms the helicity asymmetry can be large in a wider range of the driving field component intensities and for higher harmonic orders. For the stronger second field component the harmonic intensity is higher and the helicity asymmetry parameter is larger for higher harmonic orders. The results for Ne atoms are illustrated with the parametric plots of elliptically polarized attosecond high-harmonic field.

## I. INTRODUCTION

High-order harmonic generation (HHG) is a strong-laser-field-induced process in which the energy absorbed from the laser field is emitted in the form of a high-energy photon. For this process it is crucial that the electron, temporarily liberated from an atom, moves away from it, turns around and returns to the parent core to recombine with it emitting a high harmonic. This process was discovered for a linearly polarized driving laser field for which the emitted high harmonics are linearly polarized [1, 2].

For specific applications it is important to generate circularly polarized high harmonics. Such harmonics can be generated using the so-called bicircular field which consists of two coplanar counter-rotating circularly polarized fields having different frequencies [3–6]. That the harmonics generated by bicircular field are circularly polarized was confirmed in [7]. Since these harmonics have helicities which alternate between +1 and -1, by combining a group of such harmonics, instead of obtaining a circularly polarized attosecond pulse train, one obtains a pulse with unusual polarization properties (in [8] a star-like structure with three linearly polarized pulses rotated by  $120^\circ$  was predicted; this was confirmed experimentally in [9]). However, if the harmonics of particular helicity are stronger, i.e., if we have helicity asymmetry in a high-harmonic energy interval, then it is possible to generate elliptic or even circular pulse train. Such pulses can then be used to explore chirality-sensitive processes which, for example, appear in magnetic materials [10, 11], organic molecules [12, 13] etc. Fortunately, such a helicity asymmetry exists for HHG by inert gases having the  $p$  ground state [14–16].

The aim of the present work is to explore the influence of the bicircular-laser-field-component intensities on the circularly polarized high-order harmonics.

Such an analysis shows how one can control the ratio of the intensities of harmonics having opposite helicities. It should be mentioned that, in addition to HHG (see more recent Refs. [17–20]), other strong-field processes in bicircular field have been explored (for reviews see [21, 22]). Examples are above-threshold detachment [23], laser-assisted electro-ion radiative recombination [24], high-order above-threshold ionization [25–32], laser-assisted scattering [33], nonsequential double ionization [34, 35], electron vortices in photoionization [36, 37], spin-dependent effects [38], subcycle interference effects [39], attoclock photoelectron interferometry [40], high harmonics from relativistic plasmas [41], and optical chirality in nonlinear optics [42]. The results of the present paper are relevant also for these processes.

## II. THEORY

We consider an  $\omega-r\omega$  bicircular field with  $r$  integer, the fundamental frequency  $\omega = 2\pi/T$ , and the component intensities  $I_1 = E_1^2$  and  $I_r = E_r^2$ , defined by (in atomic units)

$$\begin{aligned} E_x(t) &= [E_1 \sin(\omega t) + E_r \sin(r\omega t)]/\sqrt{2}, \\ E_y(t) &= [-E_1 \cos(\omega t) + E_r \cos(r\omega t)]/\sqrt{2}. \end{aligned} \quad (1)$$

Our theory of HHG by bicircular field was presented in [16]. The intensity of the  $n$ th harmonic is defined by

$$I_n = \frac{(n\omega)^4}{2\pi c^3} |\mathbf{T}_n|^2, \quad \mathbf{T}_n = \int_0^T \frac{dt}{T} \sum_m \mathbf{d}_m(t) e^{in\omega t}, \quad (2)$$

where  $\mathbf{d}_m(t)$  is the time-dependent dipole and the magnetic quantum number is  $m = 0$  for  $s$  state or  $m = \pm 1$  for  $p$  state. Using the dynamical symmetry of the bicircular

field, one can derive the following selection rule for the  $n$ th harmonic and its ellipticity  $\varepsilon_n$ :

$$\varepsilon_n = \pm 1 \text{ for } n = q(r+1) \pm 1. \quad (q - \text{integer}) \quad (3)$$

Therefore, we can define the helicity asymmetry parameter by

$$A_{q(r+1)} = \frac{|T_{q(r+1)+1}|^2 - |T_{q(r+1)-1}|^2}{|T_{q(r+1)+1}|^2 + |T_{q(r+1)-1}|^2}. \quad (4)$$

The  $T$ -matrix element (2) is calculated in the strong-field approximation by integration over the recombination time  $t$ , with

$$\begin{aligned} \mathbf{d}_m(t) = & -i \left( \frac{2\pi}{i} \right)^{3/2} \int_0^\infty \frac{d\tau}{\tau^{3/2}} \langle \psi_{ilm} | \mathbf{r} | \mathbf{k}_{\text{st}} + \mathbf{A}(t) \rangle \\ & \times | \mathbf{k}_{\text{st}} + \mathbf{A}(t-\tau) | \mathbf{r} \cdot \mathbf{E}(t-\tau) | \psi_{ilm} \rangle e^{iS_{\text{st}}}. \end{aligned} \quad (5)$$

In (5) the integral is over the electron travel time  $\tau$  of a product of the ionization and recombination matrix elements, the electron wave-packet spreading factor  $\tau^{-3/2}$ , and a phase factor with the action  $S_{\text{st}} \equiv -I_p\tau - \int_{t-\tau}^t dt' [\mathbf{k}_{\text{st}} + \mathbf{A}(t')]^2/2$  in the exponent. Here  $\mathbf{E}(t) = -d\mathbf{A}(t)/dt$ ,  $\mathbf{k}_{\text{st}} \equiv -\int_{t-\tau}^t dt' \mathbf{A}(t')/\tau$  is the stationary momentum, and  $I_p$  the ionization potential. As in [16, 43], we model the atomic wave function  $\psi_{ilm}$  by a linear combination of the Slater-type orbitals. All presented results, except those of Fig. 3, are focal-averaged over the laser intensity distribution. In all our calculations we fix the fundamental wavelength to  $\lambda = 1300$  nm (photon energy  $\hbar\omega = 0.9537$  eV). Results are calculated for infinitely extended plane wave (CW)  $T$ -periodic laser field. It should be mentioned that for a few-cycle laser pulse the harmonic peaks are not well resolved and the results depend on the carrier-envelope phase [44]. In this case, for a bicircular field, the results also depend on the relative phase between the field components (i.e. on the time delay between the two pulses) [20].

Focal-averaging over the laser intensity is done in the following way. We suppose a Gaussian laser beam with the intensity distribution in the focus given by  $I(r, z) = I_0 (1 + z^2/z_0^2)^{-1} \exp\{-r^2/[w_0^2(1 + z^2/z_0^2)]\}$ , where  $I_0$  is the peak intensity,  $w_0$  is the minimum beam waist, and  $z_0 = \pi w_0^2/\lambda$  is the Rayleigh range. The focal averaged  $n$ th harmonic intensity is then obtained by integration over all space:  $I_n(I_0) \propto \int_{-\infty}^\infty dz \int_0^\infty r dr I_n(I(r, z))$ . From this we get

$$I_n(I_0) \propto \int_0^{I_0} dI I_n(I) \sqrt{I_0 - I} (2I + I_0) / I^{5/2}. \quad (6)$$

This focal averaging is similar to that used for electrons in ionization process. Instead of electrons we consider harmonic photons. With this focal averaging we avoid oscillations in the calculated helicity asymmetry parameter which appear for fixed intensity. This focal averaging

is an approximation since we do not take into account macroscopic effects and the harmonic phase.

In the present paper we calculate harmonic intensity using Eqs. (2) and (5). The  $T$ -matrix element is calculated by numerical integration over the times  $t$  and  $\tau$ . This two-dimensional integral over times can also be solved using the saddle-point method. This approximation leads to the quantum-orbit theory applied to HHG by bicircular field [6, 45]. We shortly introduce some elements of this theory which can be used to explain physical origin and meaning of the obtained numerical results. In this theory the  $T$ -matrix element is presented as  $T_{0n}^j = \sum_s A_s^j e^{iS_s}$ ,  $j = x, y$ , where the summation is over the solutions of the saddle-point equations for the ionization time  $t_{0s}$  and the recombination time  $t_s$ ,  $S_s$  is the corresponding action, and the amplitude  $A_s^j$  is a product of the ionization, propagation, and the recombination parts, known in analytical form. The times  $t_{0s}$  and  $t_s$  are complex and can be used to calculate two-dimensional electron trajectories and velocities projected into the real plane. Analyzing partial contributions to the harmonic intensity and the corresponding electron trajectories and velocities one can better understand the HHG process in bicircular field as it was done in Refs. [6, 45]. For the atoms with  $p$  ground state one should also take into account summation over the magnetic quantum number  $m$  and the fact that the corresponding matrix elements can be different for different values of  $m$ . In Refs. [14, 16] a large asymmetry in the  $m = \pm 1$  contributions to the harmonic intensity was used to explain the observed helicity asymmetry. An additional explanation of this asymmetry is provided in Ref. [16] using a semiclassical model in which the electron in the state  $\psi_{ilm}$  is characterized with the electron probability current density  $\mathbf{j}_m = m |\psi_{ilm}|^2 \hat{\mathbf{e}}_\phi / r$ . For HHG by bicircular field, in order to be able to return to the parent ion to recombine, the electron should have nonzero initial velocity  $v_y$ . The larger is this velocity, the lower is the probability of ionization. In the example presented in [16] it was shown that for the ground state having  $m = -1$  it is more probable that the electron at the ionization time appears with a larger initial velocity  $|v_y|$  than in the  $m = +1$  case, which explains why the ionization probability and the harmonic intensity are higher for the  $m = -1$  case. In addition, for  $m = \pm 1$  the recombination is such that the harmonic with the ellipticity  $\varepsilon_n = \pm 1$  are stronger.

### III. NUMERICAL RESULTS FOR HE ATOMS

Let us first present results for He atom having the  $s$  ground state and the ionization potential  $I_p = 24.59$  eV. Since in this case the magnetic quantum number is zero, we expect that the absolute value of the helicity asymmetry parameter is small. Namely, in [14, 16] it was shown (and explained using a semiclassical model) that the strong asymmetry between the partial harmonic intensities for particular values of the magnetic quantum

number  $m = \pm 1$  causes an asymmetry in emission of the plateau harmonics having opposite helicities.

In Fig. 1 we present focal-averaged results for the helicity asymmetry parameter [panels (a) and (b)] and the logarithm of the harmonic intensity [panels (c) and (d)] in false colors as functions of the ratio of the bicircular field component peak intensities and of the harmonic order  $n$ . The ratio  $I_r/I_1$ ,  $r = 2, 3$ , changes from 1/8 to 8, while the presented natural logarithm of this ratio,  $\ln(I_r/I_1)$ , changes from  $-2.0794$  to  $2.0794$ . For the  $\omega-2\omega$  case, presented in the upper panels (a) and (c), the cutoff of the harmonic plateau is the highest for  $I_2 \approx 2I_1$  and is above  $n = 200$ . With the decrease of the ratio  $I_2/I_1$ , the plateau length decreases as can be seen in the panel (c). This manifests as a color structure in the upper left part of the panel (a). Analogous is valid for  $I_2 > 2I_1$  and the upper right part of the panel (a). The cutoff for the  $\omega-3\omega$  case, presented in the lower panels (b) and (d), is above  $n = 160$  for  $I_3 > I_1$ . It decreases with the decrease of the ratio  $I_3/I_1$ . The mentioned change in the color structure in the panel (b) nicely follows the shape of the cutoff region (the helicity asymmetry in this region does not have a meaning since the harmonics beyond the cutoff cannot be observed). The two blue stripes in the upper right part of the panel (b) are connected with the multiplateau structure which develops in the HHG spectrum for the  $\omega-3\omega$  case. This structure can be explained using the quantum orbit theory and analyzing the corresponding partial contributions to the harmonic emission rate [45]. Namely, for  $I_3 > 4I_1$ , in addition to a plateau with the cutoff at  $n \approx 140$ , a longer plateau appears with a cutoff above  $n = 160$ . The intensity of this longer plateau is lower and it is not important for applications. The corresponding electron trajectories have shape of a square while the electron velocity during the travel time follows the shape of the vector potential [45]. Partial harmonic intensities have their own cutoffs which can be larger for longer orbits (this is contrary to the linearly polarized field case for which the shortest orbits have the highest cutoff).

What is the most important in Fig. 1 is the large helicity asymmetry for low harmonic orders. The red structures near  $n = 40$  appear both for the  $\omega-2\omega$  and  $\omega-3\omega$  cases. They are particularly noticeable for  $I_r < I_1$  and diminish for  $I_r \approx I_1$ . With the increase of the value of the ratio  $I_r/I_1$ , the helicity asymmetry for  $n < 40$  appears again. It appears earlier for the  $\omega-2\omega$  case. For the  $\omega-3\omega$  case it becomes noticeable for  $I_3 > 2I_1$ . Therefore, even using He atoms, having the  $s$  ground state, it is possible to generate highly chiral attosecond bursts by combining a group of low harmonics. This was analyzed in detail in Sec. 4 of Ref. [46] for  $I_2 = 2I_1$ . We have now shown that this effect also exists for focal-averaged spectra and for other intensity ratios. It is particularly pronounced for  $I_1 > I_r$ . Furthermore, a train of circularly polarized harmonic pulses can also be generated using  $\omega-3\omega$  bicircular field, as it follows from Fig. 1(b). However, for applications it is not enough that the helicity asym-

metry parameter is large. It is also necessary that the high-harmonic intensity is high.

In Fig. 2 we present the low-harmonic-order part of the lower panels of Fig. 1, calculated with a higher precision. We see that the intensity of harmonics for  $I_3 < 0.5I_1$  is low so that, in spite of that the helicity asymmetry parameter is large in this region, it is not important for practical application. We also see that the most important is the case of  $I_3 > 4I_1$  and the region of the harmonic order near  $n = 40$ . Therefore, strong high harmonics of order  $n > 40$  having positive helicity can be generated using  $\omega-3\omega$  bicircular field with a much stronger second field component ( $I_3 = 8I_1$ ).

Using the formalism presented in the last paragraph of Sec. II it can be shown [45] that for  $I_r \geq 2I_1$  the electron velocity at the ionization time is small, while it is large for  $I_r \leq I_1$ . The ionization probability is higher for smaller velocity and this explains why the harmonic intensity is higher for  $I_r \geq 2I_1$  than for  $I_r \leq I_1$ . Furthermore, it was found in Ref. [24] that the polarization of soft x-rays emitted in bicircular-laser-field-assisted electron-ion radiative recombination can be close to circular for low emitted x-ray photon energies and for a wide range of incident electron angles. This favors the emission of low harmonics having ellipticity  $\varepsilon_n = +1$  and large positive value of the helicity asymmetry parameter, exactly as observed in Figs. 1 and 2. An alternative explanation why the helicity asymmetry parameter can be different from zero for the  $s$  ground state was recently presented in [19]. It is based on the so-called propensity rules and an analysis of the recombination matrix element. In this paper a large helicity asymmetry parameter was noticed for the  $\omega-2\omega$  bicircular field and for higher intensity of the first component. In our paper we found this effect also for the  $\omega-3\omega$  bicircular field. Furthermore, this effect appears also for the stronger second field component. This case is more important since the corresponding harmonic intensity is higher.

#### IV. NUMERICAL RESULTS FOR NE ATOMS

For Ne atoms with the  $p$  ground state and the ionization potential  $I_p = 21.56$  eV the situation is different. In Fig. 3 we present the helicity asymmetry parameter for equal component intensities and without focal averaging. The cutoff region for the  $\omega-2\omega$  case [upper panel (a)] extends from  $n = 80$  for  $I_1 = I_2 = I = 1 \times 10^{14}$  W/cm<sup>2</sup> to above  $n = 200$  for  $I > 4 \times 10^{14}$  W/cm<sup>2</sup>. For the  $\omega-3\omega$  case [lower panel (b)] the cutoff is above  $n = 130$  for  $I_1 = I_3 = I > 4 \times 10^{14}$  W/cm<sup>2</sup>. For low harmonic orders the harmonics with the positive helicities are dominant, while for the plateau and cutoff harmonics we have the opposite situation. For low laser-field intensities the helicity asymmetry changes the sign near  $n = 50$ . The corresponding harmonic order  $n$  increases with the increase of the laser intensity and for the highest presented intensity it is  $n = 78$  for the  $\omega-2\omega$  case and  $n = 68$  for the

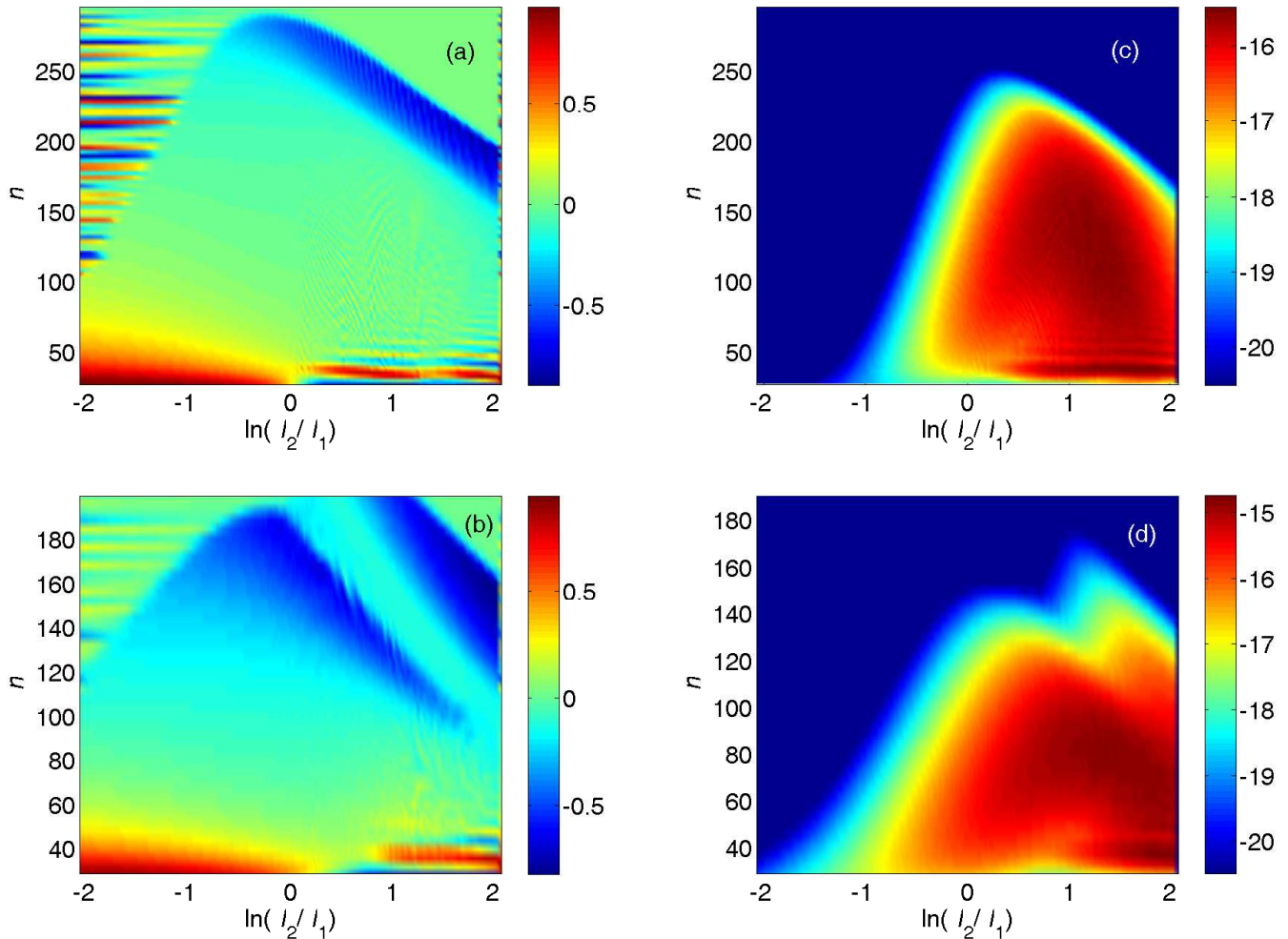


FIG. 1: Focal-averaged results for the helicity asymmetry parameter [left panels (a) and (b)] and the logarithm of the harmonic intensity [right panels (c) and (d)] for HHG by He atoms and  $\omega-2\omega$  [upper panels (a) and (c)] and  $\omega-3\omega$  [lower panels (b) and (d)] bicircular field with the fundamental wavelength 1300 nm. The results are presented in false colors as a function of the natural logarithm of the ratio of the component peak intensities,  $\ln(I_r/I_1)$ ,  $r = 2, 3$ , and of the harmonic order  $n$ . The sum of the component peak intensities is fixed to  $I_1 + I_r = 1.0 \times 10^{15} \text{ W/cm}^2$ .

$\omega-3\omega$  case. In all cases there is a wide region of the laser intensities and harmonic orders for which the asymmetry parameter is large, so that the HHG from Ne atoms can be used to explore chirality sensitive processes.

Explanation why the helicity asymmetry parameter is large for atoms having  $p$  ground state is given in Refs. [14, 16]. The reason is the asymmetry in the  $m = +1$  and  $m = -1$  contributions to the quantum-mechanical time-dependent dipole  $\mathbf{d}_m(t)$ . The asymmetry in recombination with emission of harmonics having ellipticity  $\varepsilon_n = +1$  and  $\varepsilon_n = -1$  is also important. In terms of quantum orbits, semiclassical explanation is connected with the electric ring current for atomic orbitals having  $m \neq 0$  whose sign is determined by the sign of  $m$ . As it is explained at the end of Sec. II, it is more probable that the electron appears with large velocity  $|v_y(t_0)|$  for  $m = -1$  than for  $m = +1$ , which leads

to higher ionization probability and higher partial harmonic intensity. This is the reason for the asymmetry of the  $m = \pm 1$  contributions to the harmonic intensity and for the large helicity asymmetry parameter for Ne. For lower harmonic orders, as in the case of He atoms, the recombination with emission of harmonics having the ellipticity  $\varepsilon_n = +1$  is more probable.

In Fig. 4 we explore how the helicity asymmetry parameter and the logarithm of the harmonic intensity for Ne atoms change with the change of the ratio of the bicircular field component peak intensities. The results are focal averaged and the sum of the component peak intensities is fixed to  $I_1 + I_r = 8 \times 10^{14} \text{ W/cm}^2$ ,  $r = 2, 3$ . Ratio of the peak intensities  $I_r/I_1$  changes from 1/7 to 7, i.e., the natural logarithm  $\ln(I_r/I_1)$  changes from  $-1.94591$  to  $1.94591$ . The cutoffs of the HHG spectra are clearly visible in panels (c) and (d). For low values of  $I_r/I_1$  the

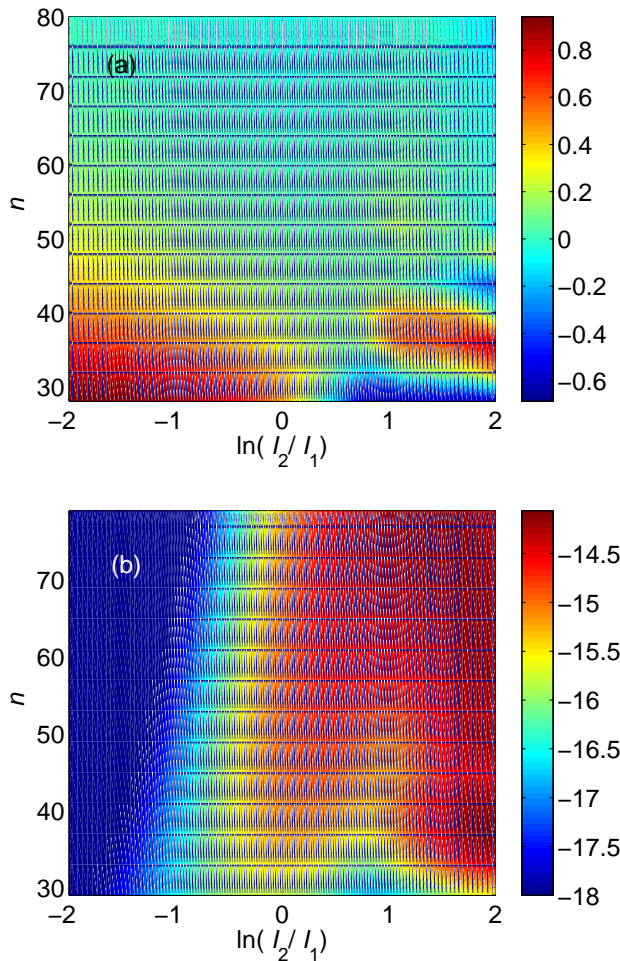


FIG. 2: Focal-averaged results for the helicity asymmetry parameter [upper panel (a)] and the logarithm of the harmonic intensity [lower panel (b)] for HHG by He atoms exposed to  $\omega-3\omega$  bicircular field, presented in false colors as a function of the natural logarithm of the ratio of the field component peak intensities and harmonic order  $n$ . Other parameters are as in Fig. 1.

HHG plateau does not develop at all, i.e., the harmonic intensity falls quickly with the increase of the harmonic order. With the increase of  $I_r/I_1$  the plateau starts to develop and for  $r = 2$  it is the longest slightly above  $I_2 = I_1$ . It is interesting that for the  $\omega-3\omega$  case the plateau is very long even for  $I_3 = 7I_1$ . For application it is important that in the region  $I_r > 2I_1$  very strong harmonics of the order  $100 < n < 150$  ( $50 < n < 90$ ) for the  $\omega-2\omega$  ( $\omega-3\omega$ ) bicircular field can be generated. From the left panels (a) and (b) of Fig. 4 we see that for  $I_r < I_1$  the harmonics having positive helicities are dominant for low harmonic orders ( $n < 50$ ). This is similar to the case of He atoms presented in Fig. 1. For Ne atoms and  $n > 50$ , the harmonics having negative helicity become dominant. With the increase of the ratio  $I_r/I_1$  the position of the zero helicity asymmetry moves to higher

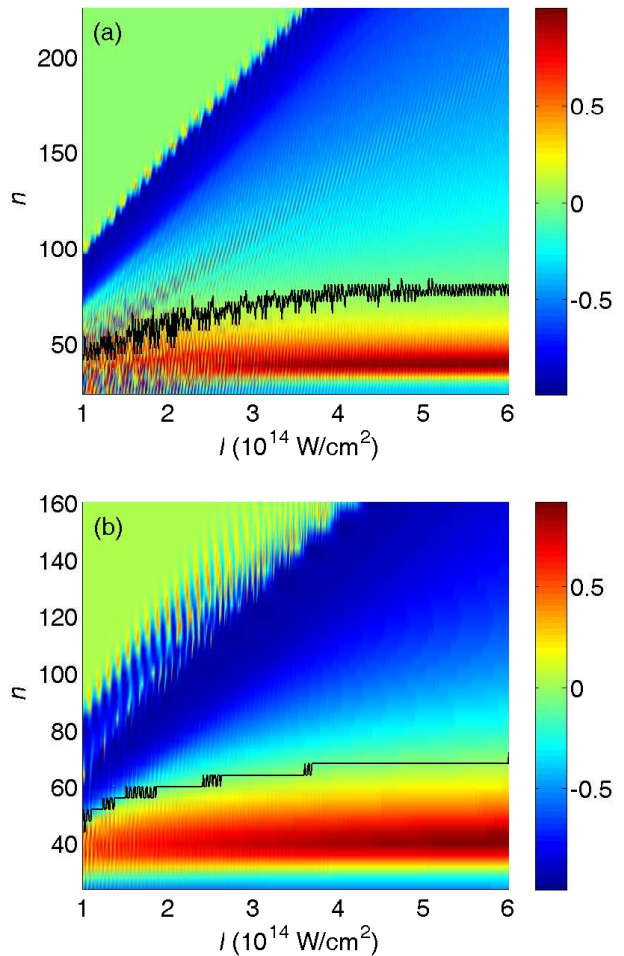


FIG. 3: Helicity asymmetry parameter presented in false colors as a function of the laser-field intensity  $I = I_1 = I_r$ ,  $r = 2, 3$ , and harmonic order  $n$  for HHG by Ne atoms exposed to  $\omega-2\omega$  [upper panel (a)] and  $\omega-3\omega$  [lower panel (b)] bicircular field with the fundamental wavelength 1300 nm. Black solid curve connects the point in which the asymmetry parameter changes the sign.

harmonic orders. For the  $\omega-3\omega$  case particularly interesting is the region of the harmonic order  $40 < n < 50$  near  $I_3 = 2I_1$ , where  $0 < \ln(I_3/I_1) < 1$ . In this region the asymmetry parameter is close to 1 and the corresponding harmonic intensity is high. With a further increase of the ratio  $I_r/I_1$ , both for the  $\omega-2\omega$  and  $\omega-3\omega$  cases, the helicity asymmetry parameter is large for a wide range of harmonic orders. Furthermore, for the  $\omega-2\omega$  case the harmonic intensity is high in the region determined by  $I_2 > 3I_1$  and  $50 < n < 150$ , while for the  $\omega-3\omega$  case the corresponding region is determined by  $I_3 > I_1$  and  $30 < n < 80$ .

In Refs. [14, 16] we have shown that, using a group of high harmonics generated by Ne atoms exposed to bicircular field, it is possible to generate elliptically polarized attosecond pulse trains. For this purpose we introduced

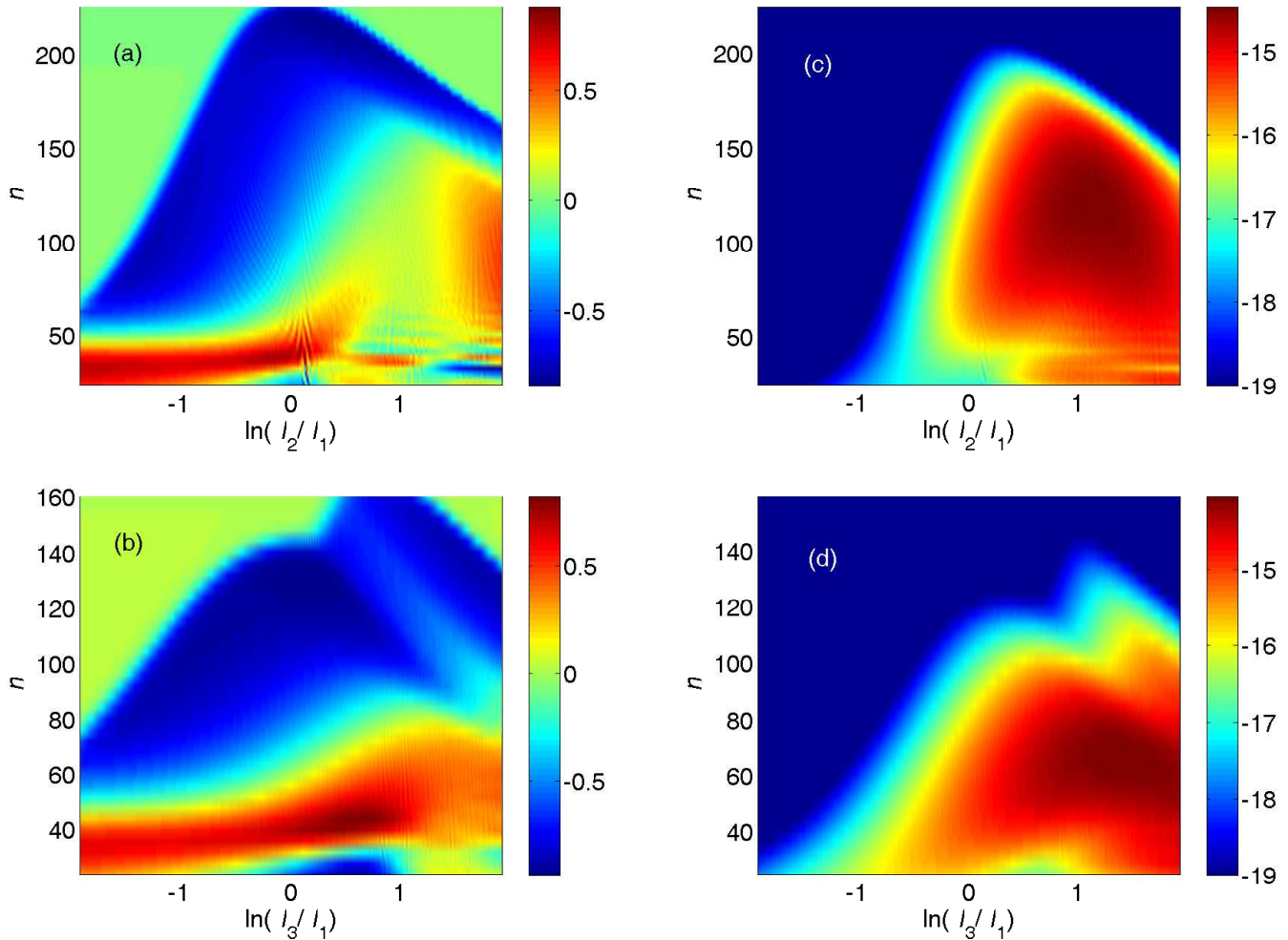


FIG. 4: Focal-averaged results for the helicity asymmetry parameter [left panels (a) and (b)] and the logarithm of the harmonic intensity [right panels (c) and (d)] for HHG by Ne atoms and  $\omega-2\omega$  [upper panels (a) and (c)] and  $\omega-3\omega$  [lower panels (b) and (d)] bicircular field with the fundamental wavelength 1300 nm. The results are presented in false colors as a function of the natural logarithm of the ratio of the component peak intensities,  $\ln(I_r/I_1)$ ,  $r = 2, 3$ , and of the harmonic order  $n$ . The sum of the component peak intensities is fixed to  $I_1 + I_r = 8 \times 10^{14}$  W/cm<sup>2</sup>.

the complex time-dependent  $n$ th harmonic electric field vector  $\mathbf{E}_n(t) = n^2 \mathbf{T}_n \exp(-in\omega t)$ , where  $t$  is the harmonic emission time, and considered the field formed by a group of subsequent harmonics from  $n = n_1$  to  $n = n_2$ . Let us now analyze such high harmonic field for different values of the bicircular field component frequencies and intensities and using focal averaging. In Fig. 5 we present, for one driving-field optical cycle  $T$ , the parametric plot of the electric field vector for various groups of harmonics. For the zero helicity asymmetry parameter we would obtain a star-like structure [8] which consists of three (for  $\omega-2\omega$  field) or four (for  $\omega-3\omega$  field) approximately linearly polarized pulses. This threefold (fourfold) symmetry reflects the corresponding symmetry of the driving field. Since in our case the helicity asymmetry parameter is different from zero we should obtain elliptically polarized attosecond pulse trains. This

is clearly visible in Fig. 5. The examples presented comprise different groups of harmonics and different ratios of the driving-field component intensities. Both the  $\omega-2\omega$  (intensities from  $I_2 = I_1$  to  $I_2 = 7I_1$ ) and  $\omega-3\omega$  (intensities from  $I_3 = I_1$  to  $I_3 = 4I_1$ ) cases are included. Since the results are presented in the same units for all panels, one can estimate the strengths of the corresponding harmonic fields for all presented examples. The harmonic field intensity is the highest for the case  $I_3 = 2I_1$  and the group of 10 harmonics from  $n_1 = 39$  to  $n_2 = 53$  ( $n = 40, 41, 43, 44, 46, 47, 49, 50, 52, 53$ ).

## V. CONCLUSIONS

In conclusion, for  $\omega-2\omega$  and  $\omega-3\omega$  bicircular fields we have explored a wide range of ratios of the bicircular

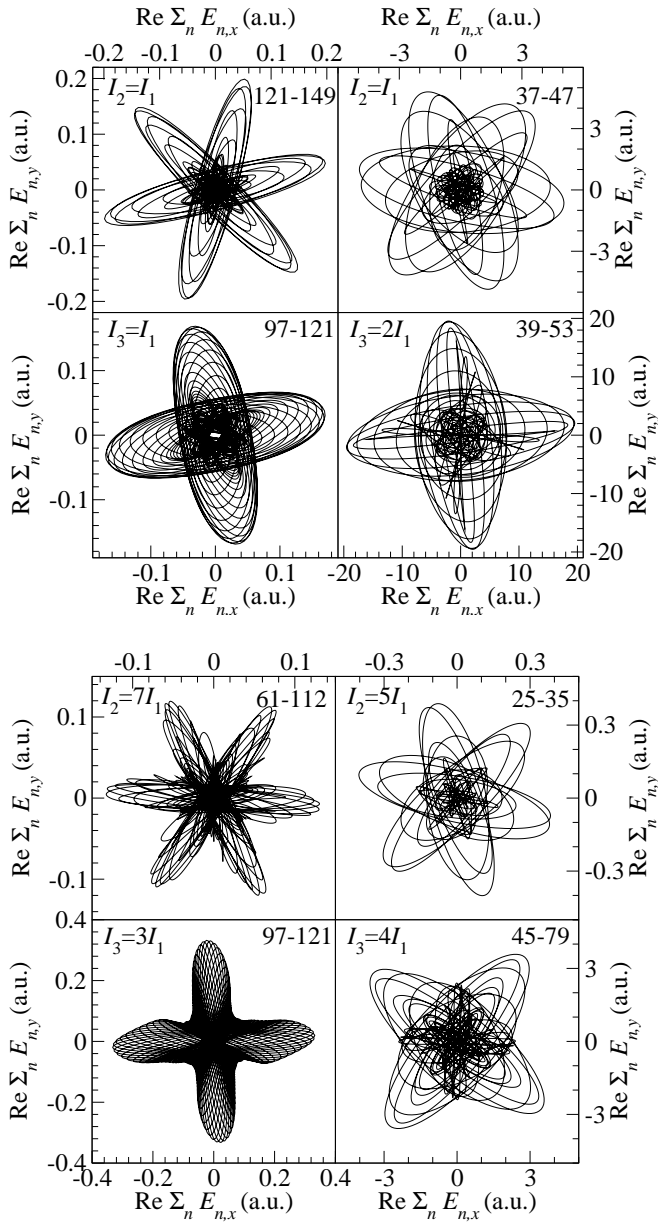


FIG. 5: Harmonic field of a group of harmonics from  $n_1$  to  $n_2$ , with the values of  $n_1$  and  $n_2$  denoted in the upper right corner of each subpanel. High harmonics are generated by Ne atoms exposed to  $\omega-2\omega$  or  $\omega-3\omega$  bicircular field. The fundamental laser wavelength is 1300 nm and the sum of the component peak intensities is fixed to  $I_1 + I_r = 8 \times 10^{14} \text{ W/cm}^2$ ,  $r = 2, 3$ . Results are presented for different ratios of the intensities as denoted in the upper left corner of each subpanel.

field component peak intensities  $I_2/I_1$  and  $I_3/I_1$  (from 1/8 to 8 for He and from 1/7 to 7 for Ne), with the goal to find the laser intensity and harmonic order regions in which the harmonic intensity is high and, at the same time, the high-harmonic helicity asymmetry parameter is large. We hope that the presented results will help the experimentalists in designing their experiments for exploration of the chirality sensitive processes.

In particular, for He atoms, having the  $s$  ground state, we have shown that strong high-order harmonics of positive helicity can be generated with the  $\omega-3\omega$  bicircular field having a much stronger second field component. For Ne atoms, having the  $p$  ground state, the helicity asymmetry parameter can be large for higher harmonic orders and in a wider range of the driving field component intensities. We confirmed that the corresponding high-harmonic pulses are elliptically polarized by presenting parametric plots of the high-harmonic field. Physical explanation of the obtained results is based on the quantum-orbit formalism.

[1] A. McPherson, G. Gibson, H. Jara, U. Johann, T. S. Luk, I. A. McIntyre, K. Boyer, and C. K. Rhodes, *J. Opt. Soc. Am. B* **4**, 595 (1987).  
 [2] M. Ferray, A. L'Huillier, X. F. Li, L. Lompré, G. Mainfray, and C. Manus, *J. Phys. B* **21**, L31 (1988).  
 [3] H. Eichmann, A. Egbert, S. Nolte, C. Momma,

B. Wellegehausen, W. Becker, S. Long, and J. K. McIver, *Phys. Rev. A* **51**, R3414 (1995).  
 [4] S. Long, W. Becker, and J. K. McIver, *Phys. Rev. A* **52**, 2262 (1995).  
 [5] T. Zuo and A. D. Bandrauk, *J. Nonlinear Opt. Phys. Mat.* **04**, 533 (1995).

- [6] D. B. Milošević, W. Becker, and R. Kopold, *Phys. Rev. A* **61**, 063403 (2000).
- [7] A. Fleischer, O. Kfir, T. Diskin, P. Sidorenko, and O. Cohen, *Nature Photon.* **8**, 543 (2014).
- [8] D. B. Milošević and W. Becker, *Phys. Rev. A* **62**, 011403(R) (2000).
- [9] C. Chen, Z. Tao, C. Hernández-García, P. Matyba, A. Carr, R. Knut, O. Kfir, D. Zusin, C. Gentry, P. Grychtol, et al., *Sci. Adv.* **2**, e1501333 (2016).
- [10] T. Fan, P. Grychtol, R. Knut, C. Hernández-García, D. D. Hickstein, D. Zusin, C. Gentry, F. J. Dollar, C. A. Mancuso, C. Hogle, et al., *Proc. Natl. Acad. Sci. USA* **112**, 14206 (2015).
- [11] O. Kfir, S. Zayko, C. Nolte, M. Sivis, M. Möller, B. Hebler, S. S. P. K. Arekapudi, D. Steil, S. Schäfer, M. Albrecht, et al., *Sci. Adv.* **3**, eaao4641 (2017).
- [12] R. Cireasa, A. E. Boguslavskiy, B. Pons, M. C. H. Wong, D. Descamps, S. Petit, H. Ruf, N. Thiré, A. Ferré, J. Suarez, et al., *Nat. Phys.* **11**, 654 (2015).
- [13] L. Nahon, L. Nag, G. A. Garcia, I. Myrgorodska, U. Meierhenrich, S. Beaulieu, V. Wanie, V. Blanchet, R. Geneaux, and I. Powis, *Phys. Chem. Chem. Phys.* **18**, 12696 (2016).
- [14] D. B. Milošević, *Opt. Lett.* **40**, 2381 (2015).
- [15] L. Medišauskas, J. Wragg, H. van der Hart, and M. Y. Ivanov, *Phys. Rev. Lett.* **115**, 153001 (2015).
- [16] D. B. Milošević, *Phys. Rev. A* **92**, 043827 (2015).
- [17] K. M. Dorney, J. L. Ellis, C. Hernández-García, D. D. Hickstein, C. A. Mancuso, N. Brooks, T. Fan, G. Fan, D. Zusin, C. Gentry, et al., *Phys. Rev. Lett.* **119**, 063201 (2017).
- [18] J. Heslar, D. A. Telnov, and S.-I. Chu, *Phys. Rev. A* **96**, 063404 (2017).
- [19] A. Jiménez-Galán, N. Zhavoronkov, D. Ayuso, F. Morales, S. Patchkovskii, M. Schloz, E. Pisanty, O. Smirnova, and M. Ivanov, *Phys. Rev. A* **97**, 023409 (2018).
- [20] M. V. Frolov, N. L. Manakov, A. A. Minina, N. V. Vvedenskii, A. A. Silaev, M. Y. Ivanov, and A. F. Starace, *Phys. Rev. Lett.* **120**, 263203 (2018).
- [21] S. Odžak, E. Hasović, W. Becker, and D. B. Milošević, *J. Mod. Opt.* **64**, 971 (2017).
- [22] A. D. Bandrauk, J. Guo, and K.-J. Yuan, *J. Opt.* **19**, 124016 (2017).
- [23] A. Kramo, E. Hasović, D. B. Milošević, and W. Becker, *Laser Phys. Lett.* **4**, 279 (2007).
- [24] S. Odžak and D. B. Milošević, *Phys. Rev. A* **92**, 053416 (2015).
- [25] C. A. Mancuso, D. D. Hickstein, P. Grychtol, R. Knut, O. Kfir, X. M. Tong, F. Dollar, D. Zusin, M. Gopalakrishnan, C. Gentry, et al., *Phys. Rev. A* **91**, 031402(R) (2015).
- [26] E. Hasović, W. Becker, and D. B. Milošević, *Opt. Express* **24**, 6413 (2016).
- [27] D. B. Milošević and W. Becker, *Phys. Rev. A* **93**, 063418 (2016).
- [28] C. A. Mancuso, D. D. Hickstein, K. M. Dorney, J. L. Ellis, E. Hasović, R. Knut, P. Grychtol, C. Gentry, M. Gopalakrishnan, D. Zusin, et al., *Phys. Rev. A* **93**, 053406 (2016).
- [29] V.-H. Hoang, V.-H. Le, C. D. Lin, and A.-T. Le, *Phys. Rev. A* **95**, 031402(R) (2017).
- [30] D. B. Milošević and W. Becker, *J. Phys. B* **51**, 054001 (2018).
- [31] M. Li, W.-C. Jiang, H. Xie, S. Luo, Y. Zhou, and P. Lu, *Phys. Rev. A* **97**, 023415 (2018).
- [32] A. Gazibegović-Busuladžić, W. Becker, and D. B. Milošević, *Opt. Express* **26**, 12684 (2018).
- [33] A. Korajac, D. Habibović, A. Čerkić, M. Busuladžić, and D. B. Milošević, *Eur. Phys. J. D* **71**, 251 (2017).
- [34] C. A. Mancuso, K. M. Dorney, D. D. Hickstein, J. L. Chaloupka, J. L. Ellis, F. J. Dollar, R. Knut, P. Grychtol, C. Zusin, D. Gentry, M. Gopalakrishnan, et al., *Phys. Rev. Lett.* **117**, 133201 (2016).
- [35] S. Eckart, M. Richter, M. Kunitski, A. Hartung, J. Rist, K. Henrichs, N. Schlott, H. Kang, T. Bauer, H. Sann, et al., *Phys. Rev. Lett.* **117**, 133202 (2016).
- [36] J. M. Ngoko Djiokap, S. X. Hu, L. B. Madsen, N. L. Manakov, A. V. Meremianin, and A. F. Starace, *Phys. Rev. Lett.* **115**, 113004 (2015).
- [37] D. Pengel, S. Kerbstadt, D. Johannmeyer, L. Englert, T. Bayer, and M. Wollenhaupt, *Phys. Rev. Lett.* **118**, 053003 (2017).
- [38] D. B. Milošević, *Phys. Rev. A* **93**, 051402(R) (2016).
- [39] S. Eckart, M. Kunitski, I. Ivanov, M. Richter, K. Fehre, A. Hartung, J. Rist, K. Henrichs, D. Trabert, N. Schlott, et al., *Phys. Rev. A* **97**, 041402(R) (2018).
- [40] M. Han, P. Ge, Y. Shao, Q. Gong, and Y. Liu, *Phys. Rev. Lett.* **120**, 073202 (2018).
- [41] Z.-Y. Chen, *Phys. Rev. E* **97**, 043202 (2018).
- [42] O. Neufeld and O. Cohen, *Phys. Rev. Lett.* **120**, 133206 (2018).
- [43] D. B. Milošević, *Phys. Rev. A* **97**, 013416 (2018).
- [44] A. de Bohan, P. Antoine, D. B. Milošević, and B. Piraux, *Phys. Rev. Lett.* **81**, 1837 (1998).
- [45] D. B. Milošević, *J. Mod. Opt.* **65**, accepted. <https://doi.org/10.1080/09500340.2018.1511862> (2018).
- [46] D. B. Milošević, W. Becker, R. Kopold, and W. Sandner, *Laser Phys.* **11**, 165 (2001).